Chemical Engineering Journal 144 (2008) 442–452

Contents lists available at ScienceDirect

Chemical Engineering Journal

journal homepage: www.elsevier.com/locate/cej

Analysis of liquid circulation in a rectangular tank with a gas source at a corner

B. Ashraf Ali, Ch. Siva Kumar, S. Pushpavanam*

Department of Chemical Engineering, IIT-Madras, Chennai-600036 (TN), India

ARTICLE INFO

Article history:
Received 18 January 2008
Received in revised form 19 June 2008
Accepted 2 July 2008

Keywords:
Bubble plume
Euler–Euler model
k–ε Turbulent
Particle Image Velocimetry
Bubble induced circulation

ABSTRACT

In this work, we investigate experimentally and numerically the hydrodynamics induced by a bubble plume introduced at a corner of a rectangular tank. Such gas–liquid flows are inherently unsteady. Particle Image Velocimetry (PIV) was used to experimentally determine transient velocity fields in the system. For this gas–liquid flow system, both the fluctuating and mean liquid velocities were determined experimentally by PIV. This technique enables us to determine velocity fields in a 2D plane. The behavior of the system was simulated in FLUENT 6.2 using a two fluid Euler–Euler model with a constant bubble size of 3 mm. Water is treated as the continuous phase and the gas bubbles are treated as the dispersed phase. The motion of the bubbles renders the flow turbulence and this effect is captured by the mixture k–ε turbulence model. Two and three-dimensional simulations were carried out to predict the flow behavior. The predictions of the time averaged flow field, turbulent intensity etc. are compared with experimental observations. We also calculate the magnitude of the turbulent viscosity from our model. For the case of corner injection of bubbles, we conclude that the velocity at a point does not show sustained periodic oscillations in time.

1. Introduction

Many processes in the chemical industry are characterized by gas–liquid flows. In order to design efficient gas–liquid contactors a thorough understanding of the flows in such two phase systems is necessary. In gas–liquid flows, usually the liquid phase is continuous and the gas phase is dispersed in the form of bubbles. These systems are extensively used as multiphase contactors and reactors in chemical, biochemical, petrochemical, fine chemical and other allied industries [1]. An advantage in these systems is that the reactant gas itself provides the required mixing of the liquid phase. Bubble column reactors are used for carrying out gas–liquid reactions such as chlorination of hydrocarbons. They also arise in fermentation and in waste water treatment [2,3]. They provide several advantages during operation such as high heat and mass transfer rates, compactness of design and low operational and maintenance costs.

In bubble column reactors, bubbles entering the bottom of a tank containing a liquid rise up due to buoyancy. They rise in the form of a plume and drag the surrounding liquid with it. This induces a circulation of the bulk liquid in the tank. The flow field is inherently unsteady in these systems due to the strong coupling between the gas and the liquid phase. This results in unsteady flow structures in the liquid phase. Since the gas is injected at a constant flow rate, the time averaged velocity field is expected to be constant in these systems. Such systems have been investigated to understand the hydrodynamic behavior and the mixing characteristics in the past [4–6]. Mixing and transport processes have to be well understood in such two phase systems especially when they sustain multiple reactions as they decide the performance of the reactor [7]. Local flow field turbulence governs the fluid mixing and must be understood to ensure an efficient design of the system. There are two approaches, the Euler–Lagrange and the Euler–Euler approach for simulating the hydrodynamics of such systems. In both approaches, the exchange of momentum through the interface needs to be modeled. This exchange occurs primarily due to the contribution of several forces, like drag, lift, virtual mass etc. [3]. Depending on the physical problem and flow regime, the relative contribution of these forces varies. It has been found that the drag and buoyancy forces are the dominant contributors in most cases and that they cannot be neglected.

Bubble column reactors have been simulated in the past for two different geometries, cylindrical [1,2,8–10] and rectangular [4,5,11–18]. Sokolichin et al. [11] compared the results obtained using both Eulerian and Lagrangian approaches. They noticed that the Eulerian approach suffers from numerical diffusion. They concluded that this was due to the fact that the gas fraction is smeared out over the entire grid in the Eulerian approach as opposed to the Lagrangian approach where the position of every bubble within the grid cell is recorded. In order to reduce numerical diffusion

* Corresponding author. Tel.: +91 44 22574161; fax: +91 44 22570509/22570545.
E-mail address: spush@iitm.ac.in (S. Pushpavanam).

1385-8947/$ – see front matter © 2008 Elsevier B.V. All rights reserved.
doi:10.1016/j.cej.2008.07.009

in the Eulerian approach, they suggested the use of higher order discretization schemes. The main conclusion of their work was that when an appropriate discretization scheme is used, there are no significant differences between the results of the Eulerian and Lagrangian approaches.

Sokolichin and Eigenberger [12] captured the periodic movement of a bubble plume using 3D simulations in conjunction with a k–ε model. Their numerical predictions were in good agreement with long time averaged results based on LDA measurements. Mudde and Simonin [13] compared the predictions of 2D and 3D simulations for a centrally injected bubble plume. They found that the oscillatory motion of the bubble plume could be predicted only with a 3D model incorporating the effects of turbulence. The periodic motion of bubble plume however could be predicted quantitatively only after incorporating the virtual mass force.

Pfleger et al. [14] analyzed the importance of bubble induced turbulence in determining the flow field. They investigated the use of a turbulent dispersion term in the continuity equation for the gas phase. However, they found that this did not have any significant influence on the results. They concluded that the effect of including gas dispersion was the same as that arising from numerical diffusion. They also concluded that the use of a turbulent dispersion term is not necessary and a 3D simulation with a mixture k–ε turbulence model was sufficient to capture hydrodynamic behavior.

Buwa and Ranade [15] experimentally measured wall pressure fluctuations and investigated dynamics of the gas–liquid flow in a rectangular bubble column. They used this to estimate the plume oscillations. The low frequency of the plume oscillation was quantified and the effect of superficial gas velocity on the oscillation of the plume was studied.

The analysis of Buwa and Ranade [15] indicates that the extra turbulence generated by the large bubbles can be neglected. Ranade and Tayalia [16] have simulated mixing in shallow bubble columns using a passive tracer and have shown that three-dimensional transient simulations are necessary to capture the hydrodynamic and mixing behavior in these systems.

The k–ε model was found to predict the mean values of velocity profiles accurately [9,17]. These predictions were compared with LES simulations in [17]. Bubble induced turbulence was not found to be significant [17]. Virtual mass force was found to have no significant effect on velocity profiles [18]. The oscillations in the plume were predicted using an Euler–Euler approach [18].

Most of the hydrodynamic studies analyzed by past researchers were for centrally injected bubble plumes (Sokolichin et al. [11], Pfleger et al. [14], Buwa and Ranade [15] and Sokolinchin et al. [19]). To our knowledge, no studies have been reported in the literature for corner injection of bubbles. This scenario occurs for example in electrolytic cells where gases are liberated at the electrodes along the walls.

In the present work, we have carried out experiments and numerical simulations with the objective of obtaining flow field information across a plane as a function of gas flow rate in a rectangular tank when gas is injected from a corner. Our objective is to analyze and compare spatiotemporal variations and flow characteristics predicted using 2D and 3D numerical techniques with the experimental results. The momentum exchange between the continuous and the dispersed phase is thought of as occurring primarily through the drag force. In our numerical simulations, the drag coefficient is modeled using the correlations proposed by Schiller and Naumann [20], Morsi and Alexander [21] and using the Symmetric Model [22]. In addition to this, we have also compared simulation predictions of turbulent intensities and eddy viscosity with experimental data.

The outline of the paper is as follows. We first describe the experimental setup and the procedure followed for obtaining experimental data. In Section 3, we discuss the model and the procedure used for numerical simulations. We then compare and discuss results of experiments with simulation predictions and finally conclude by summarizing the key findings.

2. Experimental setup

We now describe the experimental setup, experimental procedure and the methods of analysis of the experimental data. The instantaneous flow field information given by the mean and fluctuating velocities of the liquid phase is of interest. Particle Image Velocimetry (PIV) is used to obtain the experimental data. The advantage of this technique is its non-intrusive character and good resolution. The experimental results are analyzed to obtain average and the fluctuating velocity components along two lines. This quantitative information is compared with model predictions. A detailed description of the PIV technique can be found in Kompenhans et al. [23].

The experimental setup (Fig. 1) used in our studies consists of a cuboidal tank of acrylic sheet which is filled with liquid to a height of 30 cm. It has a width of 20 cm and depth of 2 cm. Air is drawn from a compressor and is passed through a bed of silica gel for drying and another bed of glass wool for filtering dust particles. It is then passed through a rotameter before it enters the tank through a porous cylinder at the lower right corner, which acts as a sparger for distributing the gas in the liquid domain. The gas rises in the form of a bubble plume. This entrains the neighboring liquid and sets up a circulation in the liquid phase. The liquid is seeded with tiny, neutrally buoyant rhodamine coated particles of Poly Methyl Meth Acrylate, PMMA ($\rho = 1000\ \mathrm{kg/m^3}$, size 10 μm).

A laser sheet with a thickness of 1 mm is formed by passing a double pulsed Nd-YAG (532 nm, 120 mJ) laser beam through an optical arrangement consisting of cylindrical and spherical lenses. The sheet illuminates the plane of interest. A CCD camera is positioned perpendicular to the plane of the light sheet to capture the light scattered from the rhodamine coated particles. The emitted light from these particles is at a higher wavelength ($\lambda = 560$ nm, red) than the incident green light ($\lambda = 532$ nm). The particles in the flow field are illuminated twice at a time interval of 1400–2100 μs. The displacement of particles in the time between the laser pulses is

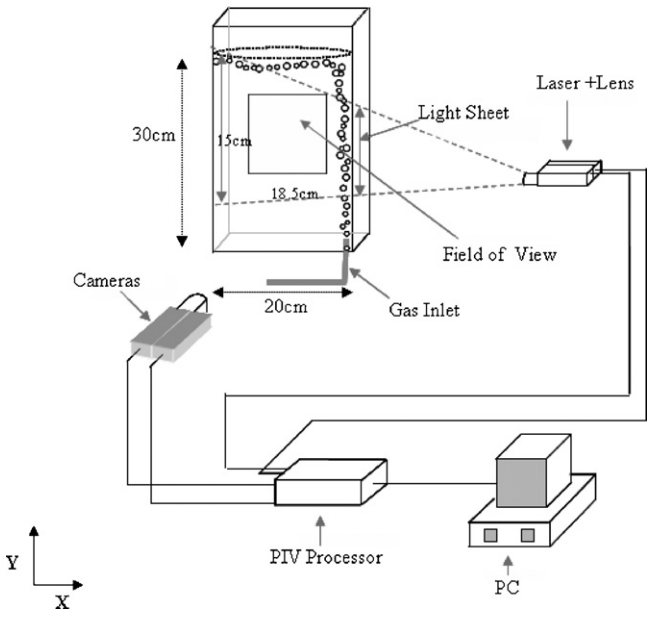

Fig. 1. Schematic representation of experimental setup.

recorded by capturing the image of the particles in each pulse. The displacement in the particle position in the image is obtained using a cross correlation technique.

The recorded particle displacement field measured across the whole field of view is scaled by the magnification of the camera and then divided by the pulse separation to obtain the velocity vector at each point. The field of view is an 18.5 cm × 15 cm region and its location is indicated in Fig. 1. For the evaluation of the liquid velocity field from the particle images it is assumed that the tracer particles follow the local flow faithfully between two illuminations. So the particle velocity directly measures the liquid velocity. An optical filter is placed in front of the camera which allows only the emitted red light from the fluorescent particles to enter the camera. The filter helps us to capture the reflection from the particles in the liquid by filtering out the unwanted green light. This helps us differentiate between the velocities of the two phases and only the liquid phase velocity is measured as only the liquid contains the fluorescent particles. Three hundred images were taken for each gas flow rate. These were processed to get the liquid velocity vector field in the entire plane.

2.1. Post processing

The images taken by the cameras are processed using DAVIS 6.2 software supplied by LAVISION GmBH to obtain the velocity vector field. There are some spurious vectors in the raw PIV velocity vector field due to noise which arises during image acquisition and processing. The spurious vectors are removed by setting an allowable vector range for the velocity components. This range is fixed after inspecting the different images. All the vectors outside this range are removed. The gaps created from the removal of vectors are filled by interpolation. Care was taken to ensure that the post-processing operation does not tamper with the flow features of the velocity field. The images were post processed using a multipass technique with progressively decreasing size of interrogation window starting from 128 × 128 pixels and going up to 32 × 32 pixels. This yields an instantaneous field of 32 × 40 vectors, i.e. total of 1280 vectors through out the field. We extract mean velocity vectors in the flow field and also the instantaneous velocity at all points for analysis and comparison with model predictions.

3. Computational model

In the present work, the flow in the bubble column reactor was modeled using a two fluid (Euler–Euler) approach using the commercial package Fluent 6.2. Here both phases are represented by their void fractions and are treated as a continuum in every infinitesimal section of the domain. The model was developed with the assumption of isothermal conditions in the tank. The liquid was taken to be incompressible and the gas density (ρ_g) was assumed to vary with local pressure as described by the ideal gas law. All the bubbles generated at the sparger are grouped into bubble classes of constant mass and the bubbles of each class retain their mass as long as they are in the computational domain. This implies that, bubble coalescence and breakage were neglected. The two phases (gas and liquid) are treated as interpenetrating continua, and the sum of the two volume fractions is taken as unity. A single pressure field is assumed to be shared by both the phases. As no mass exchange can occur between the two phases, the continuity equation (after Reynolds averaging) is formulated for the qth phase independently without any exchange term and is written as,

$$\frac{\partial}{\partial t}(\alpha_q \rho_q) + \nabla.(\alpha_q \rho_q u_q) = 0 \tag{1}$$

where u_q is the velocity, α_q is the volume fraction of phase q.

The momentum equation for the phase q (after Reynolds averaging [3,4,15,22]) is,

$$\frac{\partial}{\partial t}(\alpha_q \rho_q u_q) + \nabla.(\alpha_q \rho_q u_q u_q) = -\alpha_q \nabla p + \nabla.\tau_q + \alpha_q \rho_q g + \sum_{p=1}^{n}(k_{pq}(u_p - u_q)) \tag{2}$$

Here, the second term on the right hand side of Eq. (2) corresponds to the momentum flux due to laminar and turbulent shear stresses, the third term represents body forces and the fourth term is an interaction (drag) force between the two phases. We have neglected the effect of virtual mass and lift forces in our work.

Here, τ_q is the stress tensor of the qth phase, whose components are given by

$$\tau_q = \alpha_q \mu_q (\nabla u + \nabla u^{\mathrm{T}}) - \frac{2}{3}\alpha_q \mu_q \delta_{ij}(\nabla.u_q) \tag{3}$$

where μ_q effective viscosity of phase q.

The exchange coefficient for this gas–liquid flow can be written in the following general form,

$$k_{pq} = \frac{\alpha_q \alpha_p \rho_p f}{\tau_p} \tag{4}$$

where f=($C_D Re$/24) and τ_p is particle relaxation time which is defined as, $\tau_p = (\rho_p d_p^2/18\,\mu)$, where d_p is the diameter of the bubbles of phase p.

The Reynolds number for this flow is defined as,

$$Re = \frac{\rho_q d_p \left|u_p - u_q\right|}{\mu_q} \tag{5}$$

Using this the momentum exchange due to drag force reduces to

$$F_{\mathrm{drag}} = \frac{3}{4}(\alpha_q \alpha_p \rho_p)\frac{C_D}{d_p}(u_p - u_q)\left|u_p - u_q\right| \tag{6}$$

where C_D is drag coefficient. The evaluation of the drag coefficient requires the bubble Reynolds number which is based on the local slip velocity of a single bubble of constant diameter in a stagnant fluid. In the present computations, the drag coefficient, based on the Symmetric Model [22], and the generalized correlations of Schiller and Naumann [20] and Morsi and Alexander [21] is used.

The Schiller and Naumann [20] drag coefficient depends upon relative Reynolds number between the primary and secondary phases.

$$C_D = \begin{cases} 24(1 + 0.15Re^{0.687})/Re & Re \le 1000 \\ 0.44 & Re > 1000 \end{cases} \tag{7}$$

The drag law of Morsi and Alexander [21] is similar to the Schiller and Naumann (SN) drag law. Here the drag coefficient is given by

$$C_D = a_1 + \frac{a_2}{Re} + \frac{a_3}{Re^2} \tag{8}$$

The relative Reynolds number range is divided into eight segments. For each segment, the coefficient a_is are defined uniquely as follows:

$$a_1, a_2, a_3 = \left\{ \begin{array}{ll} 0, 18, 0 & 0 < Re < 0.1 \\ 3.690, 22.73, 0.0903 & 0.1 < Re < 1 \\ 1.222, 29.1667, -3.8889 & 1 < Re < 10 \\ 0.6167, 46.50, -116.67 & 10 < Re < 100 \\ 0.3644, 98.33, -2778 & 100 < Re < 1000 \\ 0.357, 148.62, -475000 & 1000 < Re < 5000 \\ 0.46, -490.546, 578700 & 5000 < Re < 10,000 \\ 0.5191, -1662.5, 5416700 & Re \ge 10,000 \end{array} \right\} \tag{9}$$

The drag coefficient of the Symmetric Model (SM) is a modification of the coefficient proposed by SN. Here, the exchange coefficient, k_{pq} is given by

$$k_{pq} = \frac{\alpha_p(\alpha_p\rho_p + \alpha_q\rho_p)f}{\tau_{pq}} \quad (10)$$

where,

$$\tau_{pq} = \frac{(\alpha_p\rho_p + \alpha_q\rho_q)(d_p + d_q/2)^2}{18(\alpha_p\mu_p + \alpha_q\mu_q)} \quad (11)$$

The momentum exchange term due to the drag force is written as

$$F_{\text{drag}} = \frac{3}{4}(\alpha_p\rho_q)(\alpha_p\rho_p+\alpha_q\rho_q)\frac{C_D d_p}{(d_p + d_q/2)^2}(u_p - u_q)\left|u_p - u_q\right| \quad (12)$$

where, C_D is obtained from (7).

In comparison with the drag force, the magnitude of the other two interphase forces lift and virtual mass are small. The studies of Rampure et al. [10] and Diaz et al. [18] indicate that inclusion of virtual mass force, does not result in any significant difference in dynamic and time averaged flow properties. Therefore, virtual mass force is not considered in this present work. The recent review by Sokolichin et al. [19] suggests that it is not relevant to include the lift force without any clear experimental evidence of their direction and magnitude. So, we have not included the lift force in our simulations.

Several alternatives have been proposed to estimate the effective viscosity of the turbulent liquid phase in gas–liquid two phase flows. The standard k–ε turbulence model has been reported to perform satisfactorily in such systems [3,12,14]. In the present study, to model turbulence in the gas–liquid mixture, we have used the k–ε mixture turbulence model which includes interphase turbulent momentum transfer [24,25]. Here, mixture properties and mixture velocities are used to capture important features of turbulent flow with two additional transport equations, one for the turbulent kinetic energy, k and another for the eddy dissipation rate of turbulence, ε. These are solved to compute the turbulent viscous stress tensor [26].

The transport equation for k and ε are,

$$\frac{\partial}{\partial t}(\rho_m k) + \nabla.(\rho_m u_m k) = \nabla.\left(\frac{\mu_{t,m}}{\sigma_k}\nabla k\right) + G_{k,m} + G_e - \rho_m\varepsilon \quad (13)$$

$$\frac{\partial}{\partial t}(\rho_m\varepsilon) + \nabla.(\rho_m u_m\varepsilon) = \nabla.\left(\frac{\mu_{t,m}}{\sigma_\varepsilon}\nabla\varepsilon\right) + \frac{\varepsilon}{k}(C_1[G_{k,m} + G_e] - C_{2\varepsilon}\rho_m\varepsilon) \quad (14)$$

where the mixture density and velocity ρ_m and u_m were calculated as,

$$\rho_m = \sum_{i=1}^{N}\alpha_i\rho_i \quad (15)$$

$$u_m = \frac{\sum_{i=1}^{N}\alpha_i\rho_i u_i}{\sum_{i=1}^{N}\alpha_i\rho_i} \quad (16)$$

The turbulent viscosity of the mixture, $\mu_{t,m}$, is computed from

$$\mu_{t,m} = \rho_m C_\mu\frac{k^2}{\varepsilon} \quad (17)$$

σ_k, σ_ε denotes turbulent Prandtl number for kinetic energy and dissipation rate.

$G_{k,m}$ is the generation of turbulence kinetic energy in the mixture, based on gradients of mean velocity and turbulent viscosity and is computed from,

$$G_{k,m} = \mu_{t,m}(\nabla u_m + (\nabla u_m)^T) : \nabla u_m \quad (18)$$

Following earlier studies, we have neglected the effect of G_e, the extra turbulence generation due to presence of dispersed phase [10,27]. In all the simulations, standard values of the k–ε model parameters [26] were used (C_1 = 1.44; C_2 = 1.92; C_μ =0.09; σ_k = 1.0; σ_ε = 1.3).

3.1. Numerical simulation

The behavior of the system was simulated in FLUENT 6.2 (Ansys-Fluent Inc., USA). Simulations of the fluid flow in the tank were carried out when the liquid occupied a cuboidal shape of dimensions height 30 cm, width 20 cm, and depth 2 cm. The gas inlet, located at the lower right corner of the tank, is a porous cylinder of 1 cm diameter and 2 cm height. As a first step, the flow in two dimensions was simulated and for this, the 2D domain was created using GAMBIT 2.1. The results of CFD simulations were checked for grid independence. A quad map type grid with 27,000 cells was chosen for detailed studies. A two fluid Eulerian–Eulerian model was used with a constant bubble size of 3 mm for the dispersed phase in the simulation. Water is treated as the continuous phase and gas which is in the form of bubbles is treated as the dispersed phase.

Since our interest is in transient behavior, the model equations were solved in a time-dependent mode. A time step size of 0.01 s was used in all simulations for the numerical integration. For each time step, the convergence criteria was set as the condition that the sum of normalized residuals must be less than 10^{-5}. The equations discussed above are solved in a segregated, iterative fashion and are advanced in time. At each time step, an initial guess for the pressure field was made and the primary and secondary phase velocities were calculated. These are used in the pressure correction equation (continuity equation). The velocities, holdup and fluxes are modified to get convergence in an iterative manner based on the guessed and the computed pressure field. Three-dimensional simulations of our system have also been carried out. A 3D model based on the hex map type grid with 18,750 cells was chosen for these studies. The simulation parameters, i.e. time step of integration etc., used for 3D simulations are the same as that used in the 2D model.

3.2. Boundary conditions

In the present investigation, the fraction of the bottom area where the sparger is present was modeled as a velocity inlet. The height of the static liquid column in the tank was taken to be 30 cm. Velocity of the gas in the tank was assumed to equal the rise velocity of bubbles. For a bubble of diameter 3 mm this corresponds to 0.166 m/s [28]. The superficial velocity ($U_{G,S}$) is defined as the ratio of the volumetric gas flow rate to the bottom area of the tank. The gas void fraction near the inlet at the bottom of the column was calculated using

$$\alpha_G^{in} = \frac{U_{G,S} \times \text{Area of Column}}{U_{rise} \times \text{Area of Inlet}}$$

where $U_{G,S}$ corresponds to superficial gas velocity and U_{rise} corresponds to bubble rise velocity.

Across the top surface of the liquid column, gas must escape from the tank, leaving behind a recirculating liquid. In the simulations the column is filled with liquid (water), i.e. α_l = 1; α_g = 0, up to the level that matches the static liquid height of the experiment (30 cm). Our domain of simulation is extended above this level up to a height of at least 80% of the static bed height [6]. This region

(0.24 m) is filled with gas and has the initial condition $\alpha_l = 0$; $\alpha_g = 1$. Gas is introduced at the bottom of the column and the pressure condition, i.e. the atmospheric pressure, is imposed at the top of the column at $y = 0.54$ m[0.30 + 0.24 m].

4. Results and discussion

The measurement of the velocity field in a plane was made in the rectangular tank using PIV for the gas flow rates of 2lpm and 3lpm. The area of the experimental investigation where the flow field is determined is shown in Fig. 1. The long time behavior of u and v velocity components were analyzed at $Z = 0.01$, the central plane (along the width). The instantaneous planar velocity fields were time averaged and plotted.

Fig. 2 compares the time averaged velocity field observed experimentally (Fig. 2(a)) with the model predictions (Fig. 2(b)). We observe that the velocity vectors are predominantly in the upward direction near the plume (right wall) because the liquid is dragged up by the rising gas. Away from the plume along the left wall, the velocity vectors are in the downward direction. The streamlines are in the form of closed curves in the counter clockwise direction and the flow field measured and predicted confirms this.

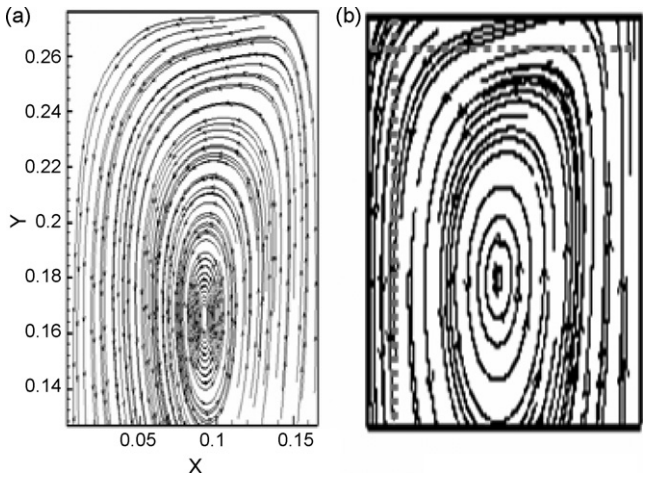

Fig. 2. Time averaged flow field in the field of view for a gas flow rate – 2lpm. (a) Experiment and (b) 2D simulation. The lines along which quantitative comparisons are made are shown in (b).

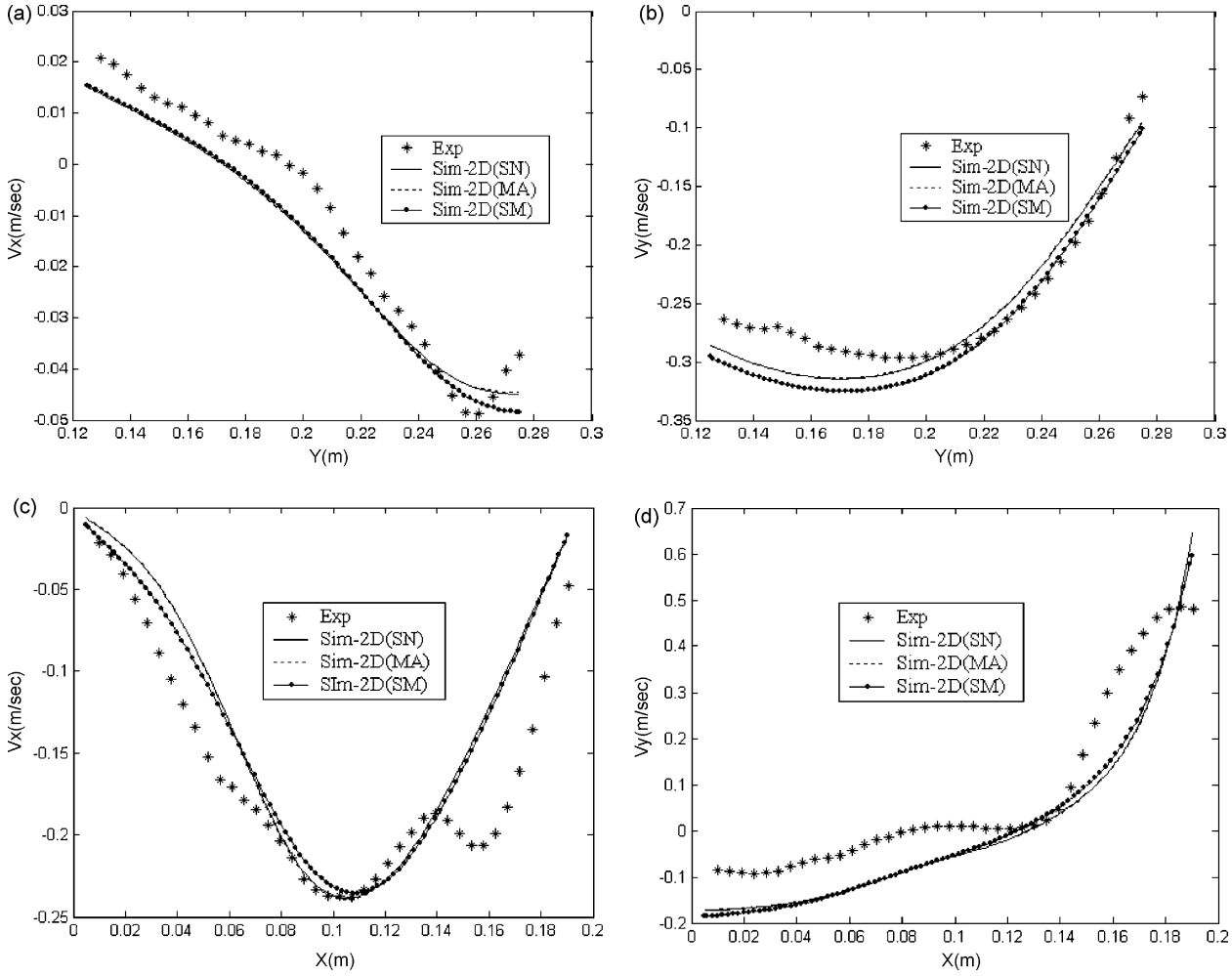

Fig. 3. Time averaged velocity along different lines. Comparison of experiments with 2D simulations using the drag coefficient proposed by Schiller and Neumann [20], Morsi and Alexander [21] and Symmetric Model [22] for a gas flow rate-2lpm. (a) Vx along $X = 0.0121$ m. (b) Vy along $X = 0.0121$ m. (c) Vx along $Y = 0.254$ m. (d) Vy along $Y = 0.254$ m.

We now proceed to make a quantitative comparison of the experimentally determined velocity vectors with the model predictions. For this, the velocity components are plotted along the horizontal and vertical lines shown in Fig. 2(b). The velocity components at a point (0.025, 0.2486) are also extracted from the instantaneous velocity fields to extract turbulent features of the flow. The origin of the coordinate system is the lower left hand corner of the tank. These are compared with model predictions.

Fig. 3(a), depicts a quantitative comparison of the time averaged *x*-component of velocity obtained experimentally with model predictions along the vertical line $X = 0.0121$ m for a gas flow rate of 2lpm, corresponding to a superficial gas velocity of 8.33×10^{-3} m/s. We observe that the velocity changes from positive to negative as we go up along the line. The velocity in the lower half is positive and in the upper half is negative, consistent with the streamlines, shown in Fig. 2.

Fig. 3(b) shows the variation of the *y*-component of velocity along the same vertical line. This is predominantly negative along the vertical line and is an order of magnitude higher than *Vx*. In Fig. 3(a and b), we depict the simulation predictions using the drag force coefficient from the Symmetric Model [22] and the correlations of Schiller and Naumann [20], Morsi and Alexander [21]. These are denoted by (SM), (SN) and (MA) respectively. We observe that the simulations using the three different methods for the drag force coefficient calculation predict the experimental data accurately.

Fig. 3(c), shows the variation of the *x*-component velocity along the horizontal line $Y = 0.254$ m. This component of velocity is always negative as the vortex is counter clockwise. Moreover, the magnitude of the velocity decreases to zero along the right and left walls where the velocity is primarily vertical. Fig. 3(d) shows the *y*-component velocity along the same horizontal line. This velocity component increases with *x*. Near the right end point, we are close to the bubble plume and the velocity is a maximum. Near the left end point the flow is primarily in the downward direction and the velocity is negative. We see that along the horizontal and vertical lines, both components of the velocities are predicted accurately by the simulations. The maximum error (point wise) is around 25%. This error is defined as the (Experimental value – Simulation Predictions)/Simulation Predictions × 100. We have also carried out experiments for a gas flow rate of 3lpm. In Fig. 4(a–d), we compare the numerical simulation predictions using the three drag coefficient models with experimental observations for this gas flow rate. We again see that the model predictions com-

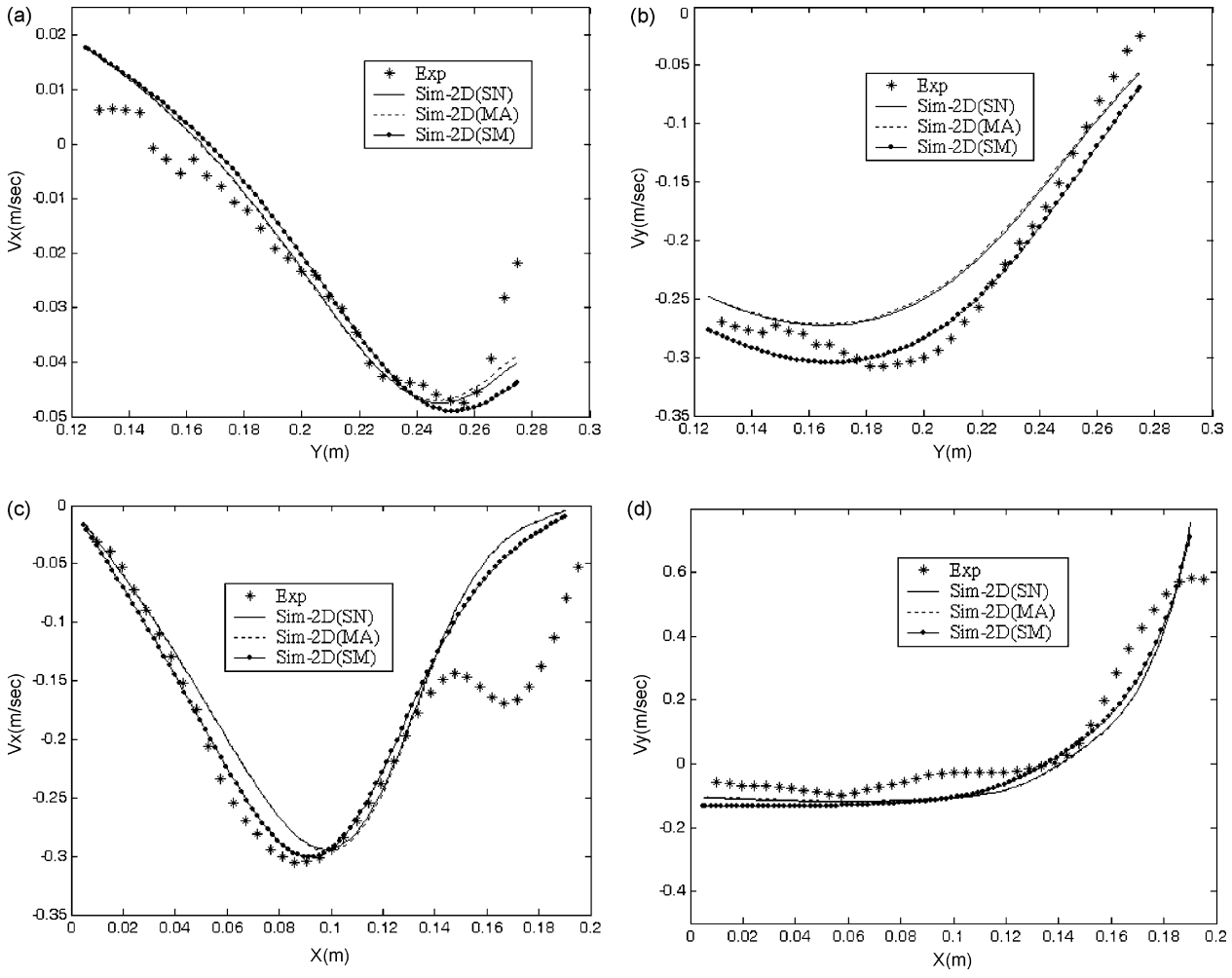

Fig. 4. Time averaged velocity along different lines. Comparison of experiments with 2D simulations using the drag coefficient proposed by Schiller and Neumann [20], Morsi and Alexander [21] and Symmetric Model [22] for a gas flow rate-3lpm. (a) *Vx* along $X = 0.0121$ m. (b) *Vy* along $X = 0.0121$ m. (c) *Vx* along $Y = 0.254$ m. (d) *Vy* along $Y = 0.254$ m.

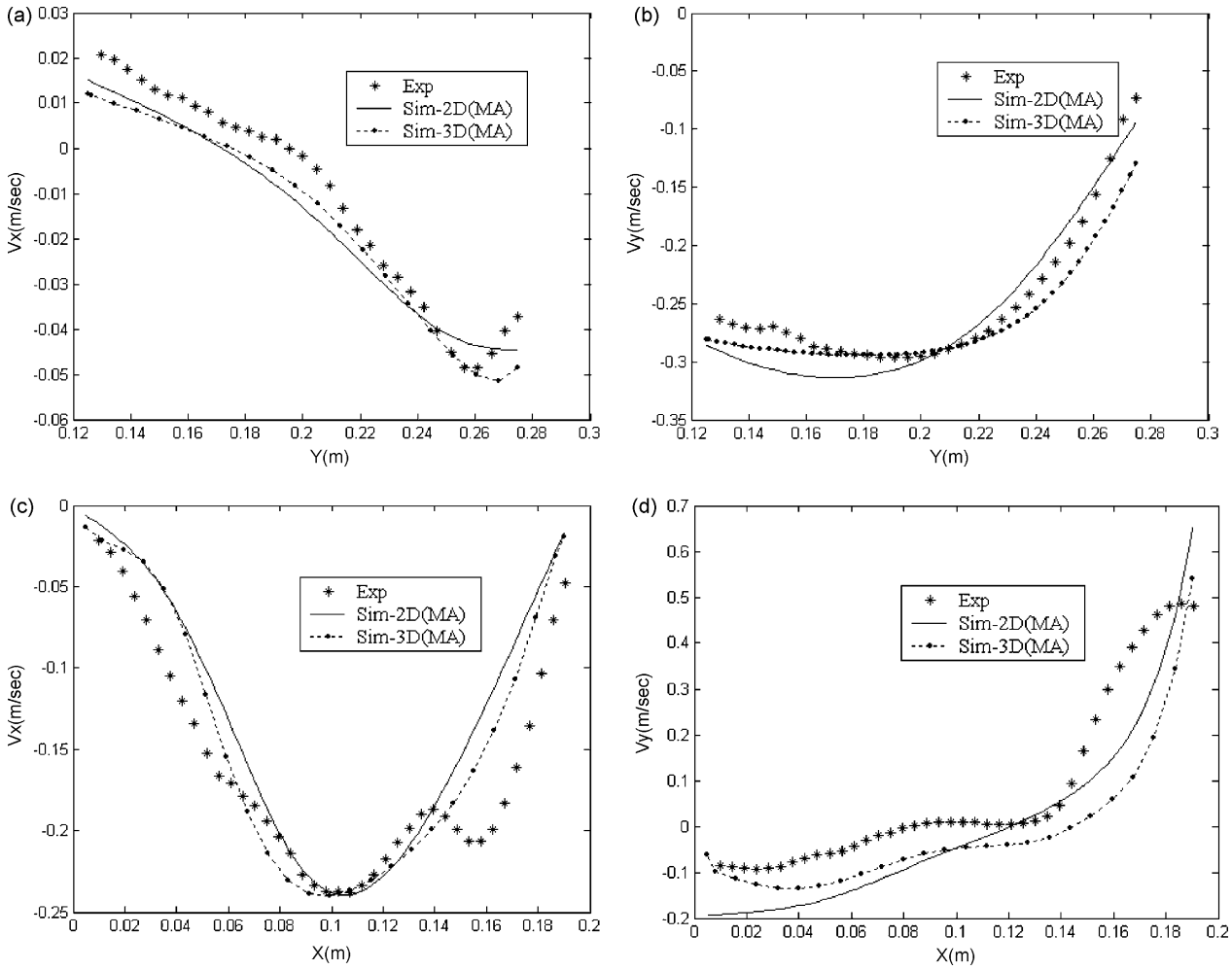

Fig. 5. Time averaged velocity along different lines. Comparison of experiments with 2D and 3D simulations for a gas flow rate 2lpm using the drag coefficient proposed by Morsi and Alexander [21]. (a) *Vx* along *X* = 0.0121 m. (b) *Vy* along *X* = 0.0121 m. (c) *Vx* along *Y* = 0.254 m. (d) *Vy* along *Y* = 0.254 m.

pare favorably to within a maximum error of around 20% (at each point) with the experimental observations in all cases. We observe that there is a good agreement of experimental data and those predicted by numerical simulations. We conclude from this that our model taking into account only the drag force can accurately predict the hydrodynamic behavior for both gas flow rates in our system.

Fig. 5(a–d) depict results of 2D and 3D simulations of liquid velocity components along the horizontal and vertical lines with experimental observations for a gas flow rate of 2lpm. We see that there is no significant change in the accuracy of the model predictions of the two components of velocity when we use a 3D model. We conclude that the quantitative velocity predictions of 2D and 3D models agree well with experimental data as far as time averaged values are concerned.

Turbulent flows are characterized by the presence of several spatial and temporal scales. Several types of flow structures are generated in these flows and these are convected by the mean flow. In turbulent flows, the velocity can be viewed as being made of a mean and fluctuating velocity, i.e. $U_{avg} + u_i'$. The average value of the fluctuating component is zero when we time average over a sufficiently long period of time [29]. So far, we have compared time average profiles along lines for validating our numerical predictions. We, now focus on estimating various temporal quantities at a point in the domain and comparing them with experimental values to further validate our model.

The Reynolds stress is a contribution to shear stress which arises from the fluctuating components of velocity when using the Reynolds-Averaged Navier-Stokes (RANS) equations [29]. It acts like additional stresses in the fluid and its effect is captured in the form of a turbulent viscosity by the two equation (mixture k–ε) model. Experimentally, the turbulent kinetic energy is calculated by $k = 1/2\ (\overline{u'^2} + \overline{v'^2})$ for a 2D flow. We can also estimate k from Eq. (5) at each point. Figs. 6 and 7 show the temporal variation of kinetic energy at a point (0.025, 0.2486). This refers to the kinetic energy of the fluid contributed by the velocity fluctuations. In Fig. 6, we see that the predictions of turbulent kinetic energy (k) using the two dimensional simulations agrees well with the experimental values for all drag coefficient models.

In Fig. 7, we have compared the predictions of the kinetic energy parameter 'k' using a 2D model as well as 3D model. We find that the 2D as well as 3D model predicts kinetic energy arising from the fluctuating velocity components. We conclude that both the 2D and 3D model predicts the temporal behavior and the turbulent characteristics of the system accurately.

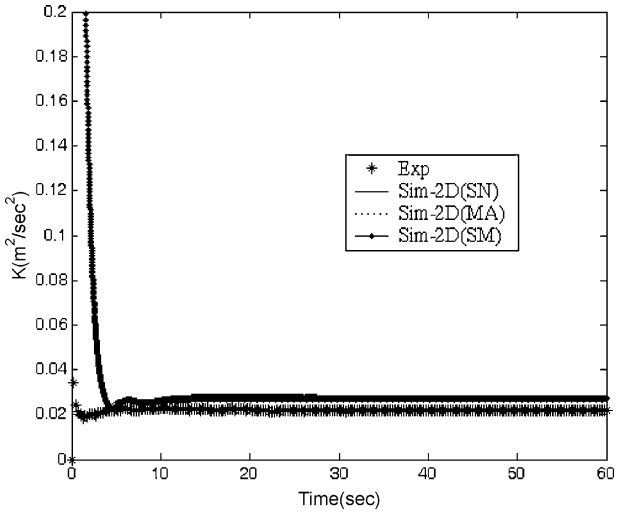

Fig. 6. Temporal Variation of Turbulent Kinetic Energy at a point (0.025, 0.2486). Comparison of experiments with 2D simulations using the drag coefficient proposed by Schiller and Neumann [20], Morsi and Alexander [21] and Symmetric Model [22] for a gas flow rate-2lpm.

Turbulence of flows is characterized by fluctuations in the flow field in space and time [30]. The instantaneous horizontal (*Vx*) and vertical (*Vy*) velocity at a point (0.025, 0.2486) was measured experimentally and are depicted in Fig. 8(a and b). It is seen that both velocity components exhibit variations in time due to turbulent fluctuations around a mean value.

Fig. 8(a and b) depicts the evolution of experimental point velocity (*Vx*) and (*Vy*) with time. The fluctuating part in these figures indicates the experimentally measured instantaneous velocity at a point in the flow. This is time averaged and compared with the time averaged prediction of the mixture k–ε turbulence model. We see that the time averaged predictions for both components compare favorably with the experimentally determined time averaged values when using a 2D model.

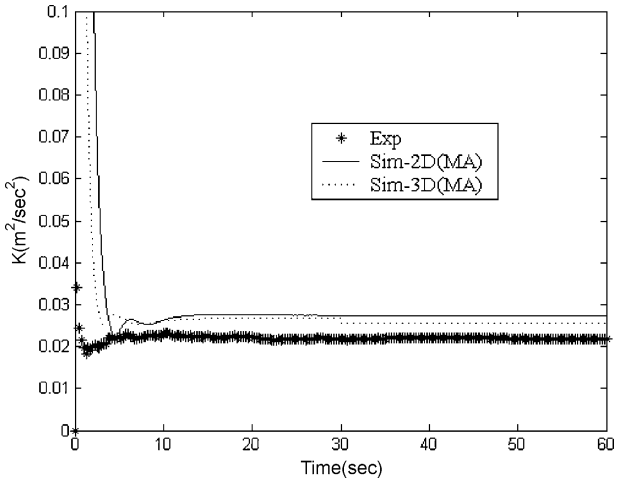

Fig. 7. Temporal Variation of Turbulent Kinetic Energy at a point (0.025, 0.2486). Comparison of experiments with 2D and 3D simulations for a gas flow rate-2lpm using the drag coefficient proposed by Morsi and Alexander [21].

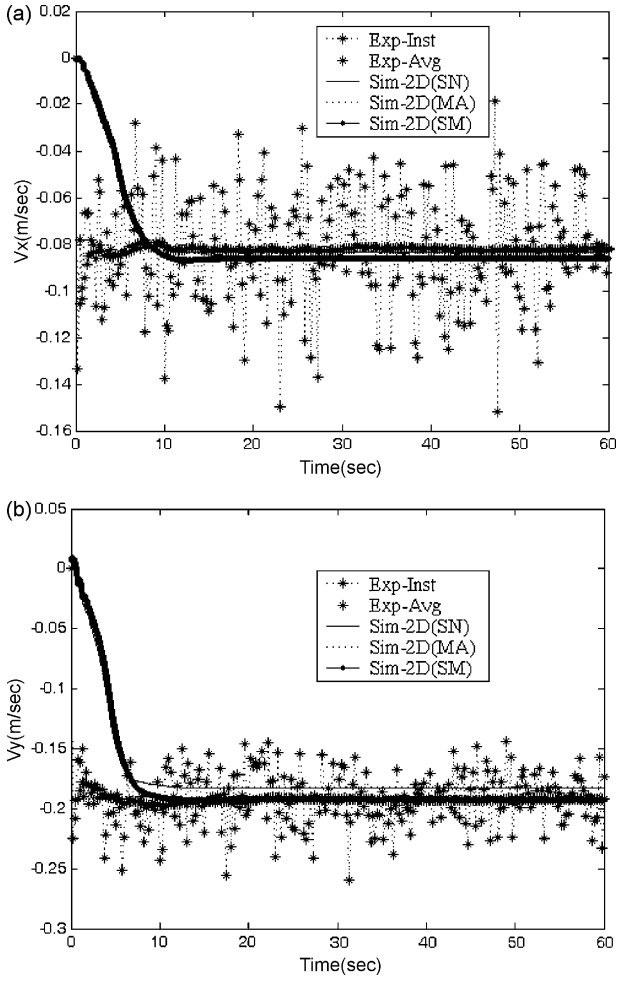

Fig. 8. Temporal variation of liquid velocity at a point (0.025, 0.2486). Comparison of experiments with 2D simulations using the drag coefficient proposed by Schiller and Neumann [20], Morsi and Alexander [21] and Symmetric Model [22] for a gas flow rate of 2lpm. (a) *Vx* and (b) *Vy*.

Fig. 9(a and b) compares the experimentally measured time averaged velocity dependence on time with 2D and 3D simulation predictions for a flow rate of 2lpm. We observe that both the 2D and 3D simulation predicts the real system behavior. From the results of point velocity measurements, we observe, after the startup period, i.e. after the initial transients have decayed, the average velocity settles at a constant value. No further change in the velocity occurs and in the time averaged sense, a steady state solution is obtained. This means that in the frame work of a k–ε turbulence model, no long term dynamic solution is achieved and we do not see any characteristic frequency in liquid velocity. This is also confirmed by experimental results.

Turbulent flows are characterized by fluctuating velocity fields. These fluctuations transport quantities such as momentum, energy etc. The frequency of these fluctuations gives us vital information about the system characteristics. The data from PIV experiments are used to analyze the frequencies present in the velocity components at a point (0.025, 0.2486) for a gas flow rate of 2lpm by power spectrum analysis. This is shown in Fig. 10(a and b). The calculations are carried out using a code written in Matlab 6.5 which uses the experimental velocity time-series data as input. It is seen that the velocity components at a point possess a wide range of

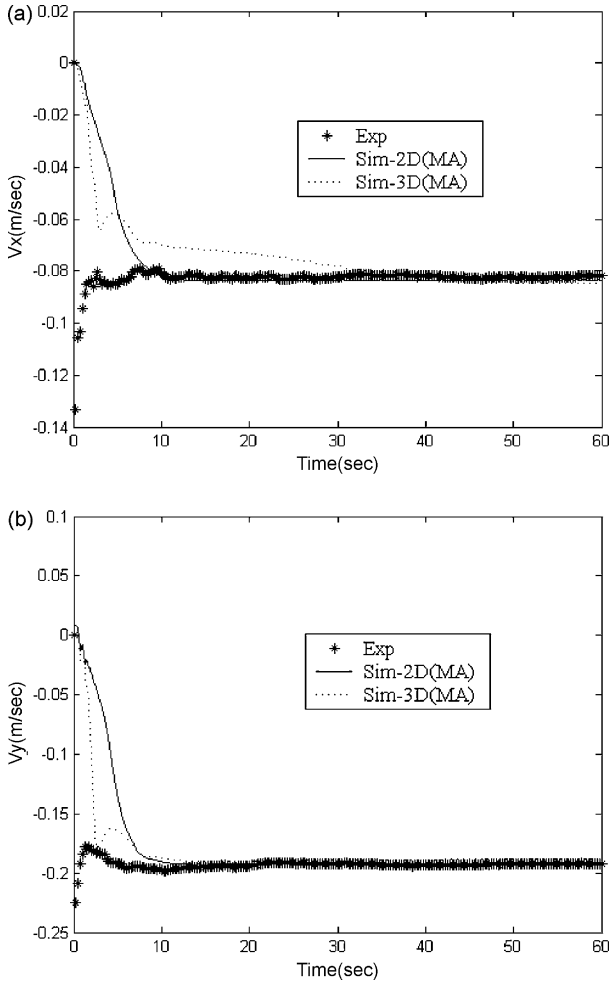

Fig. 9. Temporal variation of liquid velocity at a point (0.025, 0.2486). Comparison of experiments with 2D and 3D simulations for a gas flow rate of 2lpm using the drag coefficient proposed by Morsi and Alexander [21]. (a) *Vx* and (b) *Vy*.

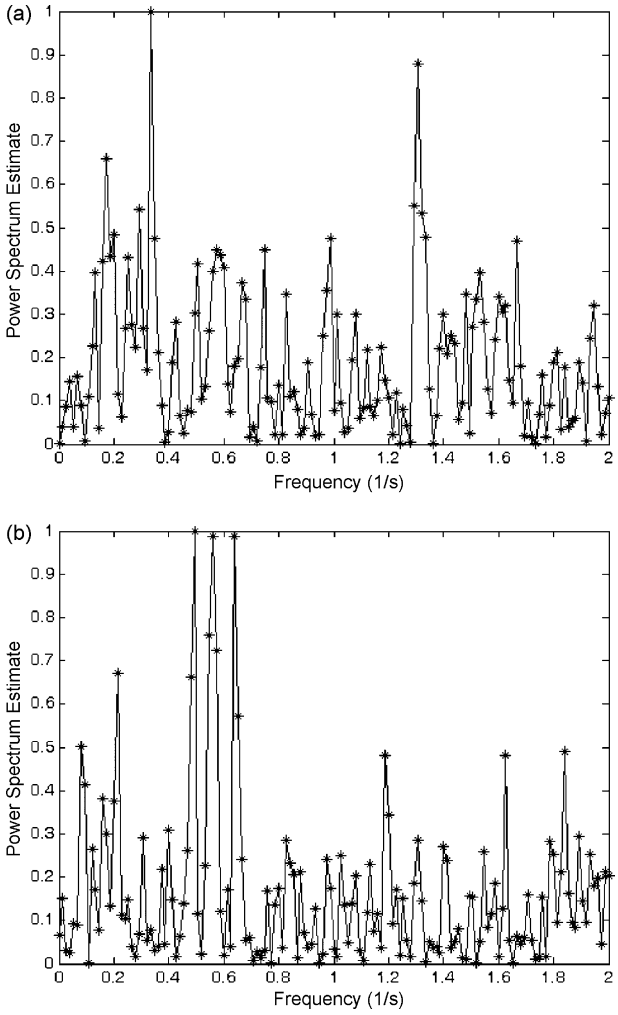

Fig. 10. Power Spectrum of Instantaneous Velocity at a point (0.025, 0.2486) for experimental observation of gas flow rate of 2lpm. (a) *Vx* and (b) *Vy*.

frequencies. From the power spectra, we conclude that the flow field has a wide range of time scales and no dominant frequencies can be observed in our experimental data confirming the turbulent nature of the flow field. In particular, there is no dominant frequency and we do not observe any oscillations in the plume or liquid velocity.

In Fig. 11, we have compared the experimentally measured as well as numerically predicted values of turbulent intensity (ratio of the RMS value to the average value) at a point. The transient evolution of this parameter is shown in the Fig. 11. We observe that, 2D and 3D model predicts same behavior in comparison with experimental observations.

We have also calculated the turbulent viscosity prevailing in our system. In our Euler–Euler two equation turbulence model, this is obtained using $\mu_t = (C_\mu \rho_l k^2/\varepsilon)$. Its spatial variation predicted from 2D and 3D simulations along a horizontal and vertical line is shown in Fig. 12. We see that the turbulent viscosity prediction by this 2D model is comparable with that predicted by the 3D model. From all results, we conclude that stationary as well as dynamic behavior are predicted equally well by the 2D and 3D models.

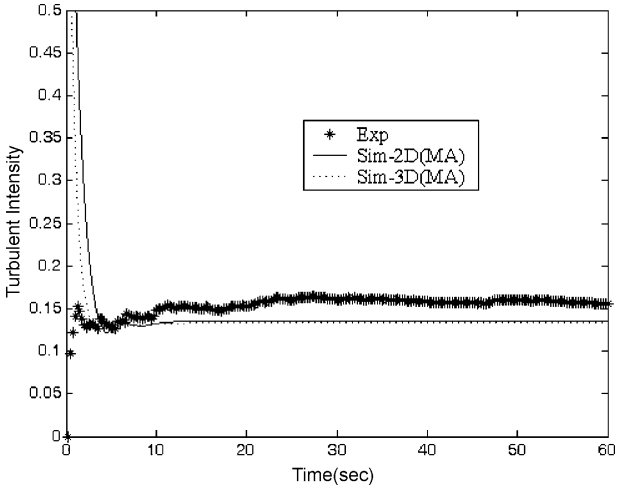

Fig. 11. Temporal variation of turbulent intensity at a point (0.025, 0.2486). Comparison of experiments with 2D and 3D simulations for a gas flow rate of 2lpm using the drag coefficient proposed by Morsi and Alexander [21].

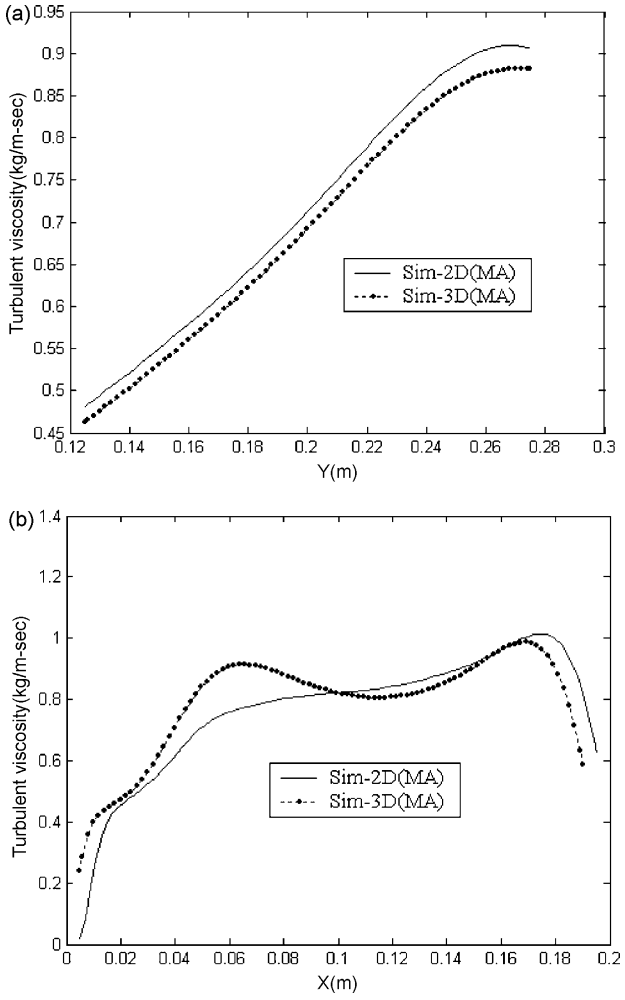

Fig. 12. Variation of turbulent viscosity along different lines. Comparison of 2D and 3D simulations for the gas flow rate of 2lpm using the drag coefficient proposed by Morsi and Alexander [21]. (a) $X = 0.0121$ m. (b) $Y = 0.254$ m.

5. Summary and conclusions

Dynamics of a gas–liquid flow in a rectangular tank induced by a bubble plume introduced in a corner was investigated by 2D and 3D CFD simulations. The predictions from simulations were compared with the experimental results obtained from PIV. Numerical simulations were carried out using an Euler–Euler approach. The mixture k–ε turbulence model is used to capture turbulence effects in the system.

Spatial variation of velocity components along horizontal and vertical lines was analyzed using 2D and 3D simulations. It was noticed that there is good agreement between the experimental results and model prediction of time average liquid velocity components along the x and y directions. Our results confirm that the drag force alone is enough to capture the gas–liquid interaction. The results of both 2D and 3D simulations with k–ε model for turbulence are in good agreement with the experimental observations as far time averaged line profiles are concerned. The hydrodynamics predicted by all three drag laws is similar. This shows the behavior is insensitive to the form of the model used for drag coefficient.

Pfleger et al. [14] observed that temporal variation of liquid velocity at a point shows periodic behavior when the bubble is injected at the center. These effects are captured only by 3D simulations and not by 2D simulations. Hence he pointed that 3D simulations are necessary to capture the real time behavior of the system. For the corner injection of the bubble, both 2D and 3D simulations show that the liquid velocity at a point do not show any oscillations or periodic flow pattern. This is also confirmed by PIV experimental results. This, we attribute to the location of sparger at the corner which damps the plume oscillations due to the column wall effects. The vertical wall near the source prevents oscillation of the plume.

The time averaged liquid velocity of 2D and 3D simulations along the x and y lines match well with experimental observations. The temporal variation of liquid velocity at a point has been considered because it connects the dispersed and the continuous phase [14]. For this, we have used the time series of point velocities and calculated the kinetic energy from the turbulent fluctuations and the turbulent intensity. This was compared with the predictions of 2D and 3D simulations. The magnitude of kinetic energy obtained experimentally agrees well with 2D and 3D simulations.

We conclude that the 2D and 3D models describe accurately the hydrodynamics in the case of a corner injection of gas in a tank. The bubble plume does not exhibit any oscillations. In a rectangular tank, with a small width, the flow structure is hence essentially 2D in nature. The plume rises straight in our experiments. This is predicted with the mixture k–ε turbulence model and is quantitatively confirmed by our PIV experimental results.

References

[1] J.B. Joshi, Computational flow modeling and design of bubble column reactors, Chem. Eng. Sci. 56 (2001) 5893–5933.
[2] D. Pfleger, S. Becker, Modeling and simulation of the dynamic flow behavior in a bubble column, Chem. Eng. Sci. 56 (2001) 1737–1747.
[3] V.V. Ranade, Computational Flow Modeling for Chemical Reactor Engineering, Academic Press, London, 2002.
[4] B. Ashraf Ali, S. Pushpavanam, Hydrodynamics of liquid circulation induced by a bubble plume, in: International Conference on Modeling and Simulation, CITICOMS, vol. I, 2007, pp. 53–58.
[5] V.V. Buwa, V.V. Ranade, Mixing in bubble column reactors: role of unsteady flow structures, Can. J. Chem. Eng. 81 (2003) 402–411.
[6] P. Chen, J. Sanyal, M.P. Dudukovic, Numerical Simulation of bubble column flows: effect of different breakup and coalescence closures, Chem. Eng. Sci. 60 (2005) 1011–1085.
[7] O. Levenspiel, Chemical Reaction Engineering, 2nd ed., Wiley, New York, 1991.
[8] A.A. Kulkarni, K. Ekambara, J.B. Joshi, On the development of flow pattern in a bubble column reactor: experiments and CFD, Chem. Eng. Sci. 62 (2007) 1049–1072.
[9] M.V. Tabib, S.A. Roy, J.B. Joshi, CFD simulation of bubble column—an analysis of interphase forces and turbulence models, Chem. Eng. J. 139 (2008) 589–614.
[10] M.R. Rampure, V.V. Buwa, V.V. Ranade, Modelling of gas–liquid/gas–liquid–solid flows in bubble columns: experiments and CFD simulations, Can. J. Chem. Eng. 81 (2003) 692–706.
[11] A. Sokolichin, G. Eigenberger, A. Lapin, A. Lubbert, Dynamic numerical simulations of gas–liquid two phase flows, Euler/Euler verses Euler/Lagrange, Chem. Eng. Sci. 52 (1997) 611–626.
[12] A. Sokolichin, G. Eigenberger, Applicability of the standard k–ε turbulence model to the dynamic simulation of bubble columns. Part I. Detailed numerical simulations, Chem. Eng. Sci. 54 (1999) 2273–2284.
[13] R.F. Mudde, O. Simonin, Two-and three-dimensional simulations of a bubble plume using a two-fluid model, Chem. Eng. Sci. 54 (1999) 5061–5069.
[14] D. Pfleger, S. Gomes, N. Gilbert, H.G. Wagner, Hydrodynamic simulation of laboratory scale bubble columns fundamental studies of the Eulerian–Euleraian modeling approach, Chem. Eng. Sci. 54 (1999) 5091–5099.
[15] V.V. Buwa, V.V. Ranade, Dynamics of gas–liquid flow in a rectangular bubble column: experiments and single/multi group CFD simulations, Chem. Eng. Sci. 57 (2002) 4715–4736.
[16] V.V. Ranade, Y. Tayalia, Modeling of fluid dynamics and mixing in shallow bubble column reactors: influence of sparger design, Chem. Eng. Sci. 56 (2001) 1667–1675.
[17] M.T. Dhotre, B. Niceno, B.L. Smith, Large eddy simulation of a bubble column using dynamic sub-grid scale model, Chem. Eng. J. 136 (2008) 337–348.
[18] M. Elena Díaz, A. Iranzo, D. Cuadra, R. Barbero, F.J. Montes, M.A. Galán, Numerical simulation of the gas–liquid flow in a laboratory scale bubble column: Influence of bubble size distribution and non-drag forces, Chem. Eng. J. 139 (2008) 363–379.
[19] A. Sokolichin, G. Eigenberger, A. Lapin, Simulation of buoyancy driven bubbly flow: established simplifications and open questions, J. Fluid Mech. Transport Phenomena 50 (2004) 24–45.

[20] L. Schiller, Z. Naumann, A drag coefficient correlation, Ver. Deutsch. Ing. (1935) 77–318.
[21] S.A. Morsi, A.J. Alexander, An investigation of particle trajectories in two-phase systems, J. Fluid Mech. 55 (1972) 193–208.
[22] Fluent 6.2, User's Guide, Fluent Inc., New Hamsphire, 2005.
[23] J. Kompenhans, M. Raffle, C.E. Willert, Particle Image Velocimetry—A Practical Guide, Springer, Berlin, 1998.
[24] B.E. Launder, D.B. Spalding, The numerical computation of turbulent flows, Comput. Methods Appl. Mech. Eng. 3 (1974) 269–289.
[25] S.E. Elghobashi, T.W. Abou-Arab, A two-equation turbulence model for two-phase flows, Phys. Fluids 26 (1983) 931–938.
[26] B.E. Launder, D. B, Spalding, Lectures in Mathematical Models for Turbulence, Academic Press, London, England, 1972.
[27] V.V. Ranade, Modeling of turbulent flow in a bubble column reactor, Chem. Eng. Res. Des. 75 (1997) 14.
[28] R. Clift, J.R. Grace, E.M. Weber, Bubbles, Drops and Particles, Academic Press, San Diego, 1978.
[29] R.B. Bird, W.E. Stewart, E.N. Lightfoot, Transport Phenomena, 2nd ed., John Wiley, New York, 2002.
[30] H. Tennekes, J.L. Lumley, A First Course in Turbulence, The MIT press, Cambridge, Massachusetts, 1987.